Radiation damage in a micron-sized protein crystal studied via reciprocal space mapping and Bragg coherent diffractive imaging

H. D. Coughlan,[1,2] C. Darmanin,[1,a)] N. W. Phillips,[1,2] F. Hofmann,[3] J. N. Clark,[4,5] R. J. Harder,[6] D. J. Vine,[6] and B. Abbey[1,7,a)]
[1]*Australian Research Council Centre of Excellence in Advanced Molecular Imaging, Department of Chemistry and Physics, La Trobe University, Melbourne 3086, Australia*
[2]*CSIRO Manufacturing Flagship, Parkville 3052, Australia*
[3]*Department of Engineering Science, University of Oxford, Oxford OX1 3PJ, United Kingdom*
[4]*Stanford PULSE Institute, SLAC National Accelerator Laboratory, Menlo Park, California 94025, USA*
[5]*Center for Free-Electron Laser Science (CFEL), Deutsches Elektronensynchrotron (DESY), Notkestrasse 85, 22607 Hamburg, Germany*
[6]*Advanced Photon Source, Argonne National Laboratory, Argonne, Illinois 60439, USA*
[7]*Melbourne Centre for Nanofabrication, Melbourne 3168, Australia*

(Received 28 February 2015; accepted 22 April 2015; published online 29 April 2015)

For laboratory and synchrotron based X-ray sources, radiation damage has posed a significant barrier to obtaining high-resolution structural data from biological macromolecules. The problem is particularly acute for micron-sized crystals where the weaker signal often necessitates the use of higher intensity beams to obtain the relevant data. Here, we employ a combination of techniques, including Bragg coherent diffractive imaging to characterise the radiation induced damage in a micron-sized protein crystal over time. The approach we adopt here could help screen for potential protein crystal candidates for measurement at X-ray free election laser sources. [http://dx.doi.org/10.1063/1.4919641]

I. INTRODUCTION

Over the past 50 years, macromolecular crystallography has been responsible for solving the structure of 100 000s of proteins. The proliferation of high intensity, third-generation synchrotron sources has enabled ever higher-resolution structures to be obtained using data collected from smaller and often more imperfect biological crystals.[1] However, with an increase in the X-ray flux incident upon the crystal comes an inevitable increase in the radiation-induced structural damage, leading to a rapid loss in diffraction intensity, particularly for the highest resolution data. Radiation damage at synchrotron and laboratory sources induces structural disorder in the crystal which affects the Bragg peaks and leads to an apparent change in unit cell dimensions reducing the probability of solving the protein structure and hindering biological interpretations.

Radiation damage is caused by the transfer of energy from the photons which comprise the illuminating X-ray beam to the crystal lattice via the photoelectric effect or inelastic scattering processes. Radiation damage can alter the protein structure through bond breaking (commonly disulfide bonds) and the creation of free radicals as well as heating. Free radicals are highly reactive species that can diffuse through the crystal and are themselves the cause of secondary

[a)]Authors to whom correspondence should be addressed. Electronic addresses: C.Darmanin@latrobe.edu.au and B.Abbey@latrobe.edu.au

damage. Whilst it is known that specific damage effects can occur prior to the diffraction pattern being visibly altered; structural damage in the crystal eventually leads to spot fading and a modification of the measured Bragg peak intensity distribution. Through early investigations of radiation damage at room temperature, it was concluded that damage was linearly proportional to the absorbed dose.[2]

Up until the 1990s, protein crystal data were collected at room temperature where, due to the higher mobility of electrons and ions, radiation damage had been a fundamental limiting factor on the resolution and quality of crystallographic data that could be collected. Large numbers of crystals were thus often required for room-temperature crystallography in order to collect a full macromolecular crystallography dataset. With the widespread availability of cryo-cooling of protein crystals[3] came a significant increase in the crystals' lifetime, this meant that in many cases, a single crystal could be used to acquire a complete crystallographic dataset. This method of cooling involves holding a crystal at a temperature of 100 K and completely surrounding the crystal with a gaseous stream of nitrogen.[4] The advantage of cryo-cooling is that the much slower diffusion rate of the secondary electrons and free radicals within the sample leads to damage being less widespread. This means that the effective dose that the crystal can tolerate before significant degradation of the diffraction intensities occurs is increased by almost two-orders of magnitude compared to room temperature samples.[5] However, in parallel to the development of cryo-cooling, the ever increasing flux available at microfocus synchrotron beamlines has permitted smaller and smaller crystal samples to be measured. With the reduced sample size, radiation damage effects can again become a significant limiting factor in data collection.[6] In addition, the recent development of 4th generation X-ray free electron laser (XFEL) sources helps to avoid the effects of structural damage altogether due to the short pulse-interactions. This opens up new possibilities for measuring damage-free structural data from micron to nano-sized crystals. Due to the limited availability of XFEL beamtime, however, it is critical to effectively screen suitable crystal targets for experiments. Frequently, the limiting factor on collecting high-quality crystallography data is not radiation damage but rather the underlying crystal quality which often cannot be overcome just by increasing the incident flux. By combining both coherent imaging and conventional rocking curve analysis for the study of micron-sized crystals, the present technique provides a novel means of selecting good candidates for further study at XFEL sources.

Protein crystals also inherently contain some level of disorder, this can manifest as rotational misalignments of small domains within the crystal volume. The crystals will also contain some resultant elastic strain distribution and surface defects, the accumulations of which are partly responsible for limiting the crystals growth. Macromolecular crystallography critically depends on the quality of the crystals used for structure determination which is largely governed by the crystallisation conditions and the growth processes of the crystal. Imperfections in the crystal lattice can directly influence the quality of structure obtained from X-ray diffraction as well as limiting the resolution of the diffraction data. During X-ray crystallography experiments, therefore, the formation of Bragg diffraction are influenced by both the intrinsic disorder of the crystal and the induced radiation damage. The combination of Reciprocal space mapping (RSM, e.g., for disorder) and Bragg Coherent Diffractive Imaging (BCDI, e.g., for size and shape) provides access to a complete range of real and reciprocal space information that can be used to characterise damage rates as well as screen crystals for growth optimisation.

RSM and 1D rocking curve analysis methods have been used to investigate crystal size and disorder effects since the earliest days of crystallography.[7,8] The effect of reducing the size of the crystal, when it is fully contained in the incident beam, is to increase the width of the Bragg peak in an identical way for every peak measured. The effect of elastic strain and the resulting asymmetries it induces in the measured diffraction meanwhile, are known to become more pronounced with increasing diffraction order.[9] From the 1980s onwards, RSM and rocking curve analysis have been extensively applied to protein crystals to study crystal perfection and radiation damage.[10–13] In order to directly study the effects of radiation damage in real space, it is possible to employ the technique of X-ray topography (XRT); however, the spatial resolution of this method is typically limited to a few microns meaning that the crystal sizes need to be of

the order of millimetres before this method can be applied effectively. For this reason, XRT could not be used to study the micron-sized protein crystals we have measured in the present work. In order to capture real space information from the crystals measured here, we used the recently developed technique of BCDI which has an intrinsically higher spatial resolution.

The availability of highly coherent X-ray sources, such as third-generation synchrotrons, has allowed the development of techniques which utilise the coherently scattered X-ray signal measured from objects in order to form a high-resolution sample image. These images have a spatial resolution, typically of the order of tens of nanometres, and also contain useful additional information about the phase of the wavefield at the exit plane of the sample. BCDI belongs to this new class of X-ray CDI methods[14] and is able to utilize the continuous diffraction signal around individual Bragg reflections to study the detailed morphology and crystalline disorder in micron and nanometer sized crystals.[15,16] In conventional crystallography, the crystal produces a diffraction pattern of discrete Bragg peaks with little to no information collected between reflections. In the case of a crystal illuminated by a sufficiently coherent beam, the crystal scatters the illumination coherently and the resultant diffracted intensity at each Bragg peak is a continuous function in reciprocal space centred around the scattering vector[17]

$$I(q) \propto \left| \int_0^\infty \rho(r) s(r) e^{iq.r} e^{iq.u(r)} dr \right|^2, \tag{1}$$

where I(q) represents the continuous intensity which is a function of q, the momentum transfer. ρ(r) is the electron density of the crystal which depends upon r, the real space coordinate; s(r) represents the shape function describing the diffracting volume and u(r) defines the relative displacements of the atoms from their ideal lattice positions.

If the intensity distribution around the Bragg peak is sufficiently well sampled[18] CDI can be used to iteratively recover both the amplitude and phase information associated with the crystals transmission function projected along the scattering vector. Although, to date, the principle applications for BCDI have been in materials science where radiation damage is minimal, one previous attempt at applying BCDI to a biological crystal was made by Boutet and Robinson.[19] In this earlier work, micron-sized protein crystals of holoferritn were measured using BCDI and their size and shape reconstructed. However, in the previous study, significant difficulties were encountered with sample stability and the radiation damage.

Here, we present the results of BCDI used to investigate radiation damage in micron-sized crystals of the protein lysozyme. By using a detector sensitive to single photons and fixation methods suitable for protein crystals, we have obtained both 3D RSM and 2D BCDI data from the crystals during interaction with a highly focused X-ray beam. As well as paving the way for coherent diffraction techniques being applied to radiation sensitive biological crystals, the data indicate that the damage mechanisms for these micron-sized crystals may differ from their macroscopic counterparts due to them being comparable in size to the typical photoelectron ranges at energies more than 6 keV.[20] This illustrates the importance of carrying out further experimental studies at this critical lengthscale and highlights the need for caution in extrapolating radiation damage characteristics established with larger crystals to crystals which are only of the order of a few microns or less in diameter.

II. METHOD

Crystals of lysozyme were grown from hen egg white obtained from Sigma-Aldrich. The tetragonal crystals have unit cell dimensions a = b = 79.1 Å, c = 37.9 Å, and space group $P4_32_12$ having eight molecules per unit cell. Protein crystals were grown in batch mode following published protocols.[21,22] A 3:1 ratio of the precipitant buffer and the protein buffer was used, giving a final protein concentration of 35 mg/ml, 4.5% PEG 6000, 13.5% (w/v) NaCl, and 0.5M acetic acid at pH 4. Crystals grew within 24 h up to a maximum dimension of $\sim 1.5 \times 1.5 \times 1.5\,\mu$m. After this time, the crystals were transferred to a storage solution

containing 9% NaCl in 0.6M acetic acid at pH 3.4 and then stored at 2 °C. The crystals were imaged for size and distribution using confocal microscopy and scanning electron microscopy (SEM).

Diffraction experiments were conducted at the undulator beamline 34-ID-C at the Advanced Photon Source (APS). A schematic of the experimental set up is shown in Fig. 1. The spatial coherence length of 34-ID-C has been previously measured as 0.66 ± 0.02 μm.[23] Protein crystals were mounted on a $10\,\mu\text{m} \times 10\,\mu\text{m}$ (400/10) MicroMeshes MiTeGen crystallography loop supported by a 18 mm copper pin and a B3S-R aluminium base (MiTeGen). A cryosolution was prepared using a 1:1 ratio of 100% glycerol stock to protein solution and loaded onto the loop by sweeping the loop through the solution multiple times. The loop was then mounted on a goniometer stage at the beamline which was modified so that a magnet capable of holding a crystallography loop at the diffractometer rotation centre could be attached. An Oxford Instruments Cryojet was set up on the stage such that it was in plane with the crystallography loop. The Cryojet produced 100 K gaseous nitrogen for flash cooling the sample. For the X-ray measurements 9 keV X-rays were focussed using Kirkpatrick-Baez (KB) mirrors to a spot measuring $2\,\mu\text{m} \times 2\,\mu\text{m}$ (full-width at half maximum, FWHM) with a total flux of 5×10^9 photons/s. The incident beam was used to illuminate areas of the mesh that were approximately perpendicular to the incident X-ray beam. A Timepix photon counting detector from the Medipix detector family with 256×256 pixels of $55\,\mu\text{m} \times 55\,\mu\text{m}$ was placed between 0.76 and 2.3 m from the sample to collect the diffraction data. The closer position was used for alignment whilst the furthest position was used to collect the BCDI data.

The Timepix detector was mounted on a diffractometer arm perpendicular to the scattering vector and an evacuated flight tube used to reduce air scatter and absorption of the diffraction signal between sample and detector. The detector arm was placed at a 2θ angle as shown in Fig. 1 for a given reflection such that the Bragg condition was satisfied. Bragg angles were between 2° and 2.5° for the (210) and (200) reflections measured for BCDI. Two types of scans were performed; a "mesh scan" to locate Bragg peaks and a rocking curve to measure a RSM of the entire Bragg peak. Mesh scans were performed by placing the detector at the Bragg angle and the near position to the sample (0.76 m) and raster scanning the sample across the X-ray beam to search for signal from individual crystals. For the RSM data, the sample crystal was rocked in θ over a total angular range of 0.5°–0.6° in increments of 0.01° with an X-ray exposure time of

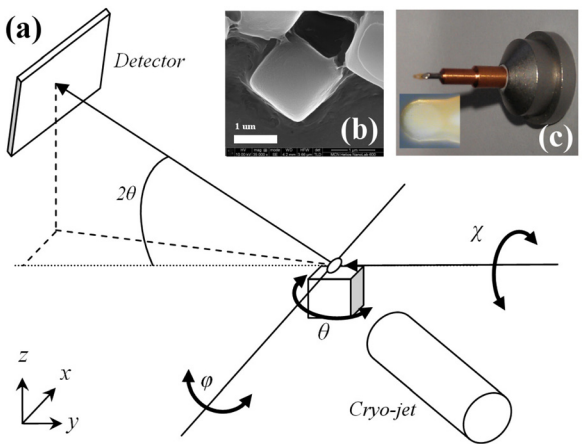

FIG. 1. Bragg coherent diffractive imaging experimental set up. (a) A schematic of the experimental set up at beamline 34-ID-C at the Advanced Photon Source with the incident photon beam on the sample and the coordinate system labeled. The angles θ, χ, and φ are the diffractometer angles used for rocking the crystal through the Bragg condition at Bragg angle, 2θ. A Timepix photon counting detector was placed 2.3 m away at the correct Bragg angle for the reflection to measure the oversampled far field diffraction pattern or at 0.76 m for alignment data. A Cryojet was placed in the x-y plane. (b) A SEM image of a representative lysozyme sample which is $1.50\,\mu\text{m} \times 1.47\,\mu\text{m}$. (c) The $10\,\mu\text{m} \times 10\,\mu\text{m}$ 400/10 MicroMeshes MiTeGen crystallography loop with an 18 mm copper pin and B3S-R aluminum base sample mount. The inset is the MicroMesh loaded with sample.

5 s per slice with the detector at a distance of 2.3 m. This process was repeated until the Bragg peak faded significantly (less than 20% of the original integrated intensity).

III. DATA ANALYSIS

In the previous work, the change in unit cell parameters has been proposed as a metric for radiation damage of protein crystals.[24] Unit cell expansion as a function of radiation dose has been examined in macroscopic protein crystals where the collection of multiple diffraction patterns forming a complete 360° dataset is feasible.[25–27] In the present case of a micron-sized crystal, where the collection of full datasets from a single crystal is not feasible, we focused on analysing the change in lattice spacing at a single orientation by examining the behaviour of a single Bragg peak. To understand the response of the crystal lattice to repeated X-ray exposure, we investigated the shift in 3D reciprocal space of the centre of mass of the Bragg peak measured at each time point. This shift was then interpreted as a change in the lattice spacing of the crystal due to radiation damage. Our reciprocal space resolution was determined to be 0.114 μm,$^{-1}$ 0.309 μm,$^{-1}$ and 0.114 μm^{-1} in x, y, and z directions, respectively, given by the configuration of the diffractometer, the wavelength of x-rays used, and the pixel size of the detector. The change in momentum transfer vector, q, was calculated and converted to an equivalent change in atomic lattice spacing, d, for the reflection as[28]

$$q = \frac{2\pi}{d} = \frac{4\pi}{\lambda}\sin\theta. \tag{2}$$

Change in integrated intensity is another method for monitoring radiation damage of protein crystals.[29] The change in integrated intensity across the entire Bragg peak was measured as a function of dose. As has been shown in the previous radiation damage work,[30] the intensity must be normalized such that the intercept on the y-axis (Fig. 5) is 1 at zero dose, i.e., the reflection intensity has not yet decreased due to radiation induced damage from the beginning of the measurement. To determine the intensity of the Bragg peak at the start of the radiation damage measurement, the integrated intensity as a function of total dose was modelled and extrapolated using a linear fit.

One benefit of measuring the full 3D Bragg reflection using a spatially resolved detector is the ability to calculate the change in width and symmetry in any direction. Here, these parameters were measured along the three orthogonal directions in reciprocal space (q_x, q_y, and q_z) which would be the equivalent of measuring rocking curves in χ, θ, and φ in Fig. 1. For χ and φ, the rocking increment was calculated, based on the detector pixel, to be 0.026°. From the rocking curves, the FWHM of the peak was determined from a Gaussian fit to the data. Using knowledge of the incident flux, X-ray wavelength, crystal size, and physical properties of the sample, the total accumulated dose the crystal received before the Bragg reflection significantly faded was 568 MGy as calculated by RADDOSE.[31] This equates to a dose per second of 0.29 MGy, higher than typical macrocrystallography beamlines due to the comparatively small focal spot size produced by the KB mirrors.

For the BCDI analysis, the central slice of each of the five 3D Bragg reflection datasets in the damage series was selected. The resulting 2D diffracted intensity data were then phased using in-house software[32] in order to recover a projection of the crystal. The programs used in the data analysis were ImageJ[33] and MATLAB. During the reconstructions, a combination of Error Reduction (ER)[34] and Relaxed Averaged Alternating Reflections (RAAR)[35] algorithms were used to retrieve the phase information. RAAR is generally able to deal with higher levels of noise in the data. In the algorithm used here, the support was updated using shrink-wrap after every 50 iterations.[36]

IV. RESULTS

Using the experimental setup, a total of 5000 images were collected using a focused beam via raster scanning across an area of 140 μm × 140 μm. Fig. 2(a) shows the sum of these images

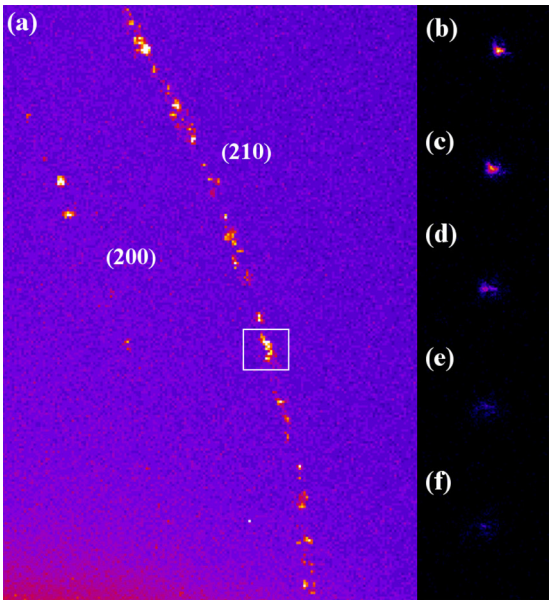

FIG. 2. Diffraction images of lysozyme: (a) The sum of ∼5000 diffraction images of micron-sized lysozyme protein crystals taken with a 2 μm × 2 μm, 9 keV focused beam. The beam was rastered across an area of 140 μm × 140 μm with the detector at 0.76 m and an exposure time of 1 s. The peaks lie on the (210) and (200) powder rings. The box indicates the position of the Bragg peak used for further analysis. Diffraction images of this Bragg peak with the detector at 2.3 m are shown after (b) 131 MGy, (c) 219 MGy, (d) 306 MGy, (e) 394 MGy, and (f) 481 MGy of dose.

measured at a sample-detector distance of 0.76 m. The closer distance was used for alignment and to determine which areas of the sample to measure for BCDI. The calculated distance between the rings was used to identify the indices of the reflection (Fig. 2). The detector was then moved to 2.3 m from the sample; for a crystal of 1.5 μm diameter at this distance, the diffraction data were oversampled, which enabled phase retrieval to be carried out. With the detector kept stationary, the crystal was rotated in the θ direction to bring it in and out of the Bragg diffraction condition.

In total, seven rocking curves were measured on the same Bragg peak of the (210) reflection for the same crystal. Diffraction images which correspond to the central slice of the Bragg peaks measured are shown in Figs. 2(b)–2(f).The measured rocking curves are shown in Fig. 3(a) as the integrated intensity in each frame of the rocking curve plotted as a function of the θ rocking angle. Figs. 3(b) and 3(c) show the calculated rocking curves in the φ and χ representing directions q_z and q_x, respectively. The first rocking curve collected was only a partial Bragg peak as the scan range was still being refined. For this reason, this rocking curve was not used in FWHM analysis but the additional dose to the sample has been taken into account in the analysis. For the Bragg peak measured, the FWHMs of the three rocking directions increased asymmetrically with a broadening factor, defined as the ratio of the final to initial FWHM, of ∼2.33 in θ, ∼1.36 in φ, and ∼1.91 in χ after 568 MGy of dose.

3D plots of five Bragg peaks measured are also shown in Fig. 3 spanning a total dose of 131–481 MGy. The first partial Bragg peak was excluded along with the last peak. Our results show that the first Bragg peak, Fig. 3(d), has a defined fringe (shown by the arrow) and central maximum. As the total dose increases (Figs. 3(e)–3(h)), the Bragg peak becomes less well-defined and moves in reciprocal space towards a lower diffraction angle. This corresponds to an increase in the *d*-spacing for this reflection of 0.06% as shown in Fig. 4. At 394 MGy, it is no longer possible to identify a clear central maximum in Fig. 3(g) and the overall maximum value in the data volume has decreased to just 11% of its initial value. The variation of *d*-spacing as a function of dose could be modelled using a logarithmic function with an R^2 quality of fit of 0.992 (Fig. 4).

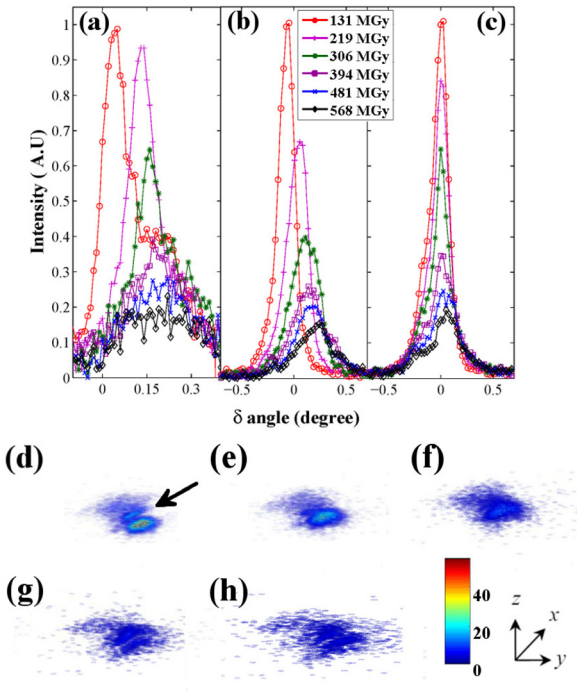

FIG. 3. Reciprocal space mapping of Bragg peaks for a micron-sized lysozyme crystal: Rocking curves are shown as integrated intensity in the three orthogonal directions of (a) θ (q_y), (b) φ (q_z), and (c) χ (q_x) after different amounts of accumulated exposure. The plots were normalized to the peak intensity. For each second of exposure, the sample received 0.29 MGy of dose. The rocking curves were plotted as a 3D volume with reciprocal space resolution was 0.114 μm^{-1}, 0.309 μm^{-1}, and 0.114 μm^{-1} after accumulated dose of (d) 131 MGy, (e) 219 MGy, (f) 306 MGy, (g) 394 MGy, and (h) 481 MGy.

The change in the Bragg peak is also reflected in Fig. 5 where as dose increases the integrated intensity of the Bragg peaks decreases. The first 5 measurements of the normalised integrated intensity as a function of total dose were modelled using a linear function with an R^2 quality of fit of 0.995. The last three points were modelled also using a linear function with an R^2 quality of fit of 0.994. The gradient was found to change dramatically from 0.18% of the intensity decreasing per second to 0.07% of the intensity decreasing per second at 400 MGy dose.

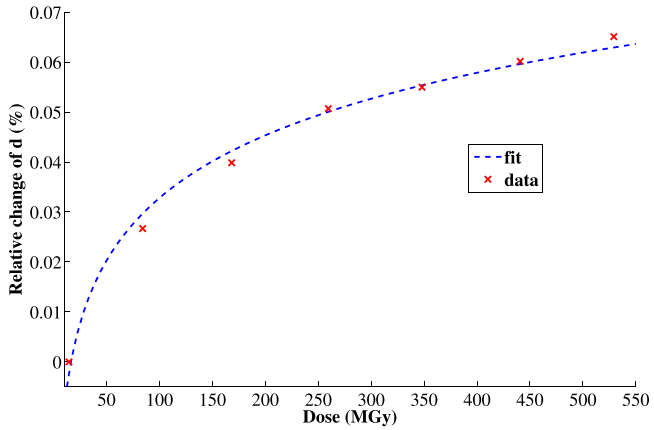

FIG. 4. Relative change of atomic lattice spacing verses dose: Relative change in atomic lattice spacing, d, of the (210) Bragg peak from a micron-sized lysozyme protein crystal is shown with respect to the increase in dose. For each second of exposure, the crystal receives a dose of 0.29 MGy. The data were fitted to a logarithmic function of *fit* $y = 0.0181\ log(Dose) - 0.0504$ with $R^2 = 0.9921$. The calculated error for the data is too small to be observed on this plot.

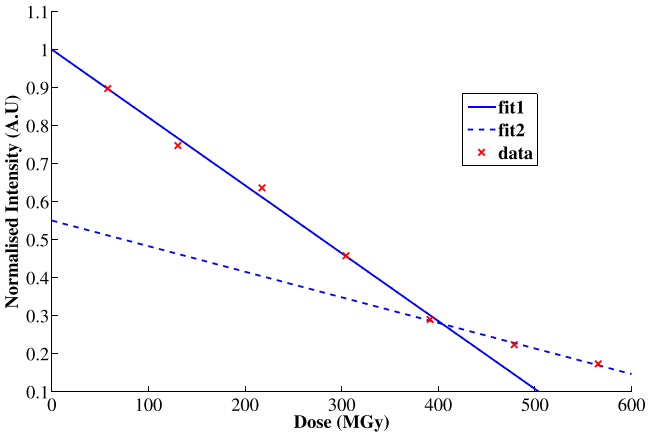

FIG. 5. Integrated intensity of Bragg peaks versus dose: Relative change in integrated normalised intensity of the (210) Bragg peak from a micron-sized lysozyme crystal changing with dose. The first five data points were fitted to a linear of fit $y = 1 - 0.0018*(Dose)$ with $R^2 = 0.995$ and the last three data points were fitted to a linear fit $y = 0.05501 - 0.0007*(Dose)$ with $R^2 = 0.994$.

Oversampled diffraction patterns were recorded whilst rocking the crystal which can be iteratively phased using BCDI techniques to give the complex density. If u(r) in Eq. (1) is non-zero, the resulting intensity distribution around the Bragg peaks is no longer centro-symmetric; asymmetries in the Bragg reflection are therefore indicative of the presence of strain within the crystal. Reconstructions of the amplitude, which can be interpreted as the crystals electron density, corresponding to 5 diffraction images of different dose (Figs. 2(b)–2(f)) are shown in Figs. 6(a)–6(e). The diffraction images also correspond to the central slice of the Bragg peak reciprocal space map (Figs. 3(d)–3(h)).

From these real-space images, the initial size of the crystal was determined to be $\sim$500 nm $\times$ 800 nm, smaller than the maximum crystal size of 1.5 μm $\times$ 1.5 μm determined by the SEM data. The size of the crystal, which was calculated using the built-in edge-detection function in MATLAB decreases, as a percentage of the original area, from 90% (after 130 MGy) to 46% (after 390 MGy) as shown in Fig. 7 with the corresponding change in FWHM in θ. After 480 MGy, the intensity of the Bragg reflection has reduced to the point, where it is no longer possible to clearly resolve any fine structure in the Bragg peak, hence

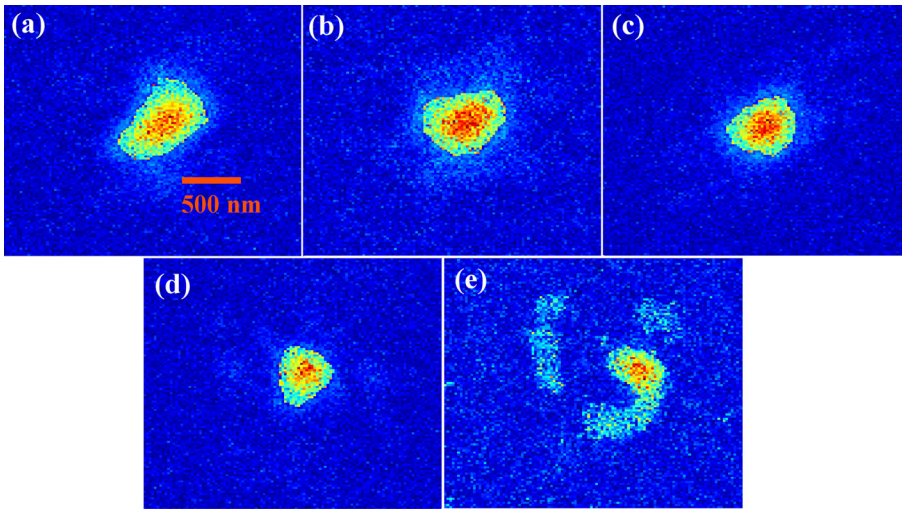

FIG. 6. Reconstructed amplitudes of diffraction patterns of the lysozyme crystal as shown in Figs. 2(b)–2(f). The 2D reconstructed amplitude from the (initially) 500 $\times$ 800 nm lysozyme protein after (a) 131 MGy, (b) 219 MGy, (c) 306 MGy, (d) 394 MGy, and (e) 481 MGy of dose. The orange scale bar corresponds to 500 nm.

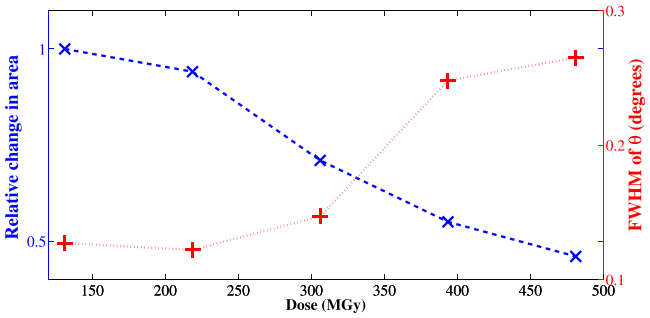

FIG. 7. Effect of X-ray dose on the micron-sized lysozyme crystal: On the left axis, the relative change in area of the reconstructed amplitude of the lysozyme crystal changing is shown as a percentage with respect to dose. On the right axis, the FWHM of the rocking curve in θ (q_y) is shown as a function of dose on the crystal.

the BCDI reconstruction failed. Interestingly, the crystal exhibits a sudden decrease in size at 400 MGy, which matches exactly the point at which there is a reduction in the rate of spot fading observed in Fig. 5.

V. DISCUSSION

Recent studies have highlighted the importance of size effects in radiation damage studies. This has partly been motivated by the recent availability of XFEL sources which have enabled measurements of diffraction data from nanocrystals.[22] In the case of XFELs, using photons of energy in the kilo electron volt range for protein crystallography means that the mean free path of photoelectrons ejected during the primary interaction may be comparable to or larger than the crystal itself.[37,38] It has been argued that in this case the radiation induced damage to the crystal may actually be reduced since the photoelectrons can escape to the surface prior to giving up all of their energy in initiating secondary damage processes.[39] Similar types of size effects have been observed at the synchrotron where the use of micron-sized beams has been shown to result in crystallographic data with a reduced damage signature due to the primary photoelectron ranges being larger than the beam footprint on the sample.[30] In the present case, we have carried out the first synchrotron radiation damage study on crystals whose dimensions are comparable to the primary photoelectron escape depth at the relevant X-ray energies. The key scientific question is whether the damage behaviour of such samples is similar to the macroscopic crystal case or whether, as has been predicted theoretically,[30] the small crystal size imparts additional radiation tolerance to the sample. To address this question, we have looked at several different metrics such as the damage effect on unit cell parameters, crystal quality, and crystal size. Analysing these three metrics provide insights in to the effect of dose on the protein crystal structure.

Perhaps the most well-established method of examining crystal quality and ordering is to analyse the FWHM of the Bragg peak. In both macroscopic and micron-crystals,[40] the FWHM has been found to increase as a function of dose.[12] For a crystal where the spatial coherence length is comparable to or larger than the crystal (as in the present case), the Bragg peak intensity distribution depends upon the complex shape function and deformation within the crystal as described in Eq. (1). A single crystal of lysozyme has approximately 39% solvent by weight; during interaction with the energetic X-ray photons, protein-solvent bonds are broken and the solvent channels within the crystal are emptied. As the crystal dries out the molecules rearrange to minimise the damage induced strain; this in turn leads to the formation of further defects with manifests as a broadening of the Bragg peak.

In our data, we examined the FWHM of the Bragg reflection in three orthogonal directions in reciprocal space (θ, φ, and χ shown in Fig. 1) and found an increase in all three directions as a function of the absorbed dose. The lysozyme crystal has a $P4_32_12$ space group which is asymmetric with respect to the crystallographic directions. This may explain the rate of peak broadening which showed a directional dependence within the sample. This asymmetric damage behaviour has been explained previously as being due to variations in the orientation of the

solvent channels within the crystal. Due to non-alignment between channels, it has been postulated that dehydration occurs at different rates in different directions and thus the creation of defects leading to peak broadening occurs anisotropically across the crystal. In macroscopic crystals, direct experimental evidence for this has been obtained through analysis of X-ray topography images.[12]

In addition to the overall broadening, the fine structure of the Bragg peak intensity can also be used to infer crystal quality. In the q_x direction, for example, there is a breaking of symmetry of the Bragg peak as the dose increases. Such asymmetries in Bragg peak shape are thought to arise, not directly due to dehydration, but rather from the formation and propagation of dislocations and cracks within the crystal.[12] In one damage model proposed by Blake and Phillips (1962),[2] it was hypothesised that under the influence of radiation induced damage, crystals decompose into highly ordered domains separated by disordered and completely amorphous regions. It has been shown experimentally that whilst diffraction from the ordered regions preserves the intensity at the original Bragg peak position, the disordered regions tend to diffract at lower angles resulting in a characteristic shoulder in the Bragg reflection. We see clear evidence of such a shoulder forming in some of the data presented in Fig. 3.

The overall position of the Bragg peak can also provide insights into radiation induced damage. In the data presented here, the results show that the lattice spacing corresponding to the (210) Bragg peak increases as a function of the total dose absorbed. Similar trends have been observed in the literature for macroscopic protein crystals. In the macroscopic case, the expansion of d-spacing with dose has been found to follow a linear relationship[28] or an exponential relationship.[41] The origin of this expansion may also be understood in terms of dehydration of the crystal which results in the repulsion of residues within the protein crystal. Rather than a linear behaviour, the rate of lattice expansion in our experiment follows a logarithmic trend (Fig. 4). Initially, up to a total dose of ~174 MGy, the lattice expands rapidly by 0.04% of the nominal value after which the rate of expansion slows down such that the lattice spacing only increases by a further 0.02% up to 350 MGy. A possible explanation for this is that the initial rapid expansion occurs as molecules rearrange to minimise strain; however, as dehydration of the crystal continues, the remaining molecules are less free to move resulting in ever smaller changes in the lattice constant. This process coincides with an increase in the levels of disorder within the crystal which reduces the intensity (shown in Fig. 5) and visibility of the measured Bragg peaks.[4] The decrease in integrated intensity as a function of dose was expected to be exponential[29] yet this was not the case. The exponential decay describes the decay of an average Bragg peak and realistically the intensity can decay in different paths depending on protein composition with one of the most pronounced changes to intensity caused by disulfide bond breakage.[42] Lysozyme has four intramolecular disulfide bonds[43] therefore has the potential for large structural damage as it undergoes radiation damage. The large change in the gradient of Fig. 5 could also be a consequence of the change in shape of the crystal which is seen in the BCDI reconstructions. As the crystal decreases in size, the photoelectrons are more likely to escape from the crystal volume potentially decreasing the radiation damage and therefore the rate of intensity loss.

Real-space analysis, which permits a direct visualisation of the change in crystal size and shape with dose, was carried out using BCDI. The reconstructed crystal was found to be smaller than the SEM data indicated which could be an artefact of the SEM sample preparation process which required the crystal to be coated with a thin (nominally 10s of nm) layer of gold. In addition the standard deviation of the sizes of crystals measured using SEM was found to be 200 nm in each linear dimension so it could be that this particular crystal was at the smaller end of the size distribution. Finally during alignment we estimate the crystal received at least ~84 MGy of dose prior to the first BCDI image being reconstructed. This known dose has been taken into account in the quantitative analysis but not in the crystal size analysis which could account for the difference we see since the crystal has already undergone some dehydration before the first BCDI datasets were collected. The BCDI results clearly indicate the crystal volume is decreasing as a result of the radiation damage. As far as the authors are aware such radiation damage effects have not been directly studied in real-space before. The reciprocal and real space data can also be directly correlated; one example of this is shown in Fig. 7

where the decrease in area of the crystal was reflected in the broadening of the FWHM in θ (Fig. 7). As the reciprocal data indicated, the size and shape of the crystal change in a way which is direction dependant. With the crystal initially shrinking fastest along the longest axis producing a more or less symmetrical shape towards the end. After 394 MGy, the diffracted signal became too low for BCDI to be carried out reliably.

Compared to small-molecule, radiation hard materials science samples, BCDI of crystals made of biological macromolecules is extremely challenging. The crystals need to be hydrated and the dynamically evolving sample size and shape, captured here, mean that data need to be collected quickly and extreme care needs to be taken in optimising the fixation conditions. Nonetheless, despite the amount of scatter being significantly reduced compared to their materials counterparts, our data prove that with modern synchrotron sources and photon-sensitive detection, BCDI of protein crystals is feasible and can provide a wealth of additional information that complements the reciprocal space analysis. Future experiments will investigate whether any changes are observed with increased beam conditioning to improve the coherence length. Another issue is the signal-to-noise (SNR); due to limitations in the diffracted signal, we estimate the spatial resolution of the measurement to be $\sim$90 nm based on the numerical aperture of the detected scatter, sufficient to resolve the crystals size and shape but not sufficient to really resolve the internal features. Improvements in the sample preparation and delivery will help improve the signal in comparison to the background, in particular, minimising the amount of surrounding solution prior to freezing will reduce the broad diffuse background scatter due to the buffer and cryo-protectant solutions.

For our experiments, we found one of the most significant challenges to be the motion of the crystals during data collection. Because they are not adhered directly to the substrate many of our earlier experiments were unsuccessful due to sample drift and rotation during data collection. Extensive studies were carried out examining the effect of sample stability and drift of the protein crystals during BCDI measurements. The effectiveness flash freezing fixation was tested at both 34-ID-C and the MX2 beamline at the Australian Synchrotron, where Bragg peak stability was monitored over comparable periods of time to determine if crystals were translating or rotating within the beam. During these investigations, we found many stable crystals and therefore concluded that this type of sample fixation was the suitable for BCDI experiments.

VI. CONCLUSION

Radiation damage in a micron-sized protein crystal has been examined using a combination of reciprocal space mapping and BCDI techniques. The additional information provided by real-space images of the crystal as it undergoes dehydration and apparently shrinks in the beam aids in the interpretation of the diffraction data where the convolution of reciprocal and real space information can make separating out the various factors contributing to the measured diffraction intensity challenging. Following on from published protocols, we have carried out an analysis of the intensity, position and shape of the Bragg peak collected from a micron-sized protein crystal. The increase in FWHM is clearly matched by shrinking of the crystal in real-space. The reduction in crystal volume, the increase in disorder, and the breaking of bonds all contribute to the significant loss of intensity we observe. Experimental radiation damage data published from macroscopic crystals usually shows a linear increase in d-spacing with dose, this trend is not observed here with micron-sized crystals. We find that the rate of change of the d-spacing is initially significantly higher with the initial exposure compared to later on and that the variation of in d-spacing actually most closely follows a logarithmic trend. The rate of decrease of the normalised intensity for the (210) reflection also appears to reduce significantly at around 400 MGy. The evidence from the reciprocal space analysis therefore points to a slowing down of the radiation damage processes as a function of dose, the same behaviour is not observed in macroscopic protein crystals.

The reduction in the rate of radiation damage with dose can be understood by considering the real-space images of the crystal as it undergoes dehydration. Following the arguments of, e.g., Sanishvili *et al.*[30] and Holton *et al.*[29] lessening of the expected damage rates for micron

and sub-micron crystals may be interpreted as a reduction in the amount of induced secondary damage within the diffracting crystal volume. Since the crystal studied here was smaller than the average stopping range of the primary ejected photoelectrons we interpret the reduction in damage rates to be due to the in-situ shrinking of the crystal size. As can be seen from the BCDI measurements, even early on in the measurement the well-ordered parts of the crystal dynamically changes size and shape with increasing dose. We hypothesised that during the damage process the reduction in diffracting crystal volume actually aids in preserving the crystal longer in the beam than might otherwise be expected.

In conclusion, if confirmed, the dynamical reduction of radiation damage with shrinking crystal volume could have significant benefits for crystallography carried out using micron and sub-micron sized crystals at third-generation synchrotrons. BCDI experiments, even on ideal materials science samples, can often be challenging. However, through the pilot experiment reported on here, we have demonstrated that this technique can be applied successfully to radiation sensitive biological crystals. The real-space analysis we have carried out here of the dynamically evolving crystal size as a function of dose will be followed up with additional measurements, first to confirm this behaviour for a statistically significant number of protein crystals and secondly for higher order reflections at diffraction resolutions typically used for crystallography. Nonetheless, the results of combining newly developed coherent imaging techniques with reciprocal space analysis for micron-sized crystals are intriguing and, we are confident, pave the way for BCDI becoming an effective tool for characterising and understanding the growth, structure, and diffraction properties of protein crystals.

ACKNOWLEDGMENTS

The software implementation of the phase retrieval algorithms used in this work was developed by J. N. Clark. Use of the Advanced Photon Source was supported by the U.S. Department of Energy, Office of Science, Office of Basic Energy Sciences, under Contract No. DE-AC02-06CH11357. Part of this research was undertaken on the MX1 and MX2 beamlines at the Australian Synchrotron, Victoria, Australia. With the help and expertise of Eugeniu Balaur, this work was also performed in part at the Melbourne Centre for Nanofabrication (MCN) in the Victorian Node of the Australian National Fabrication Facility (ANFF). This work was partly funded by the CSIRO Materials Science and Engineering Capability Development Fund. The work was carried out in collaboration with the ARC centre of excellence in Coherent X-ray Science and the ARC centre of excellence in Advanced Molecular Imaging. J. N. Clark gratefully acknowledges financial support from the Volkswagen Foundation.

[1]J. R. Helliwell, "Synchrotron X-radiation protein crystallography: Instrumentation, methods and applications," Rep. Prog. Phys. **47**, 1403 (1984).
[2]C. C. Blake and D. C. Phillips, "Effects of X-irradiation on single crystals of myoglobin," in *Biological Effects of Ionizing Radiation at the Molecular Level* (International Atomic Energy Agency, Vienna, 1962), p. 183.
[3]H. Hope, "Cryocrystallography of biological macromolecules: A generally applicable method," Acta Crystallogr. Sect. B **44**, 22 (1988).
[4]E. F. Garman, "Radiation damage in macromolecular crystallography: What is it and why should we care?," Acta Crystallogr. Sect. D **66**, 339 (2010).
[5]C. Nave and E. F. Garman, "Towards an understanding of radiation damage in cryocooled macromolecular crystals," J. Synchrotron Radiat. **12**, 257 (2005).
[6]B. Ziaja, H. N. Chapman, R. Fäustlin, S. Hau-Riege, Z. Jurek, A. V Martin, S. Toleikis, F. Wang, E. Weckert, and R. Santra, "Limitations of coherent diffractive imaging of single objects due to their damage by intense x-ray radiation," New J. Phys. **14**, 115015 (2012).
[7]M. Laue, "The external shape of crystals and its influence on interference phenomena in crystalline lattices," Ann. Phys. **26**, 55 (1936).
[8]T. Ino and N. Minami, "X-ray diffraction by small crystals," Acta Crystallogr. Sect. A **35**, 163 (1979).
[9]T. J. Boggon, R. A. Judge, A. Olczak, and E. H. Snell, "Synchrotron X-ray reciprocal-space mapping, topography and diffraction resolution studies of macromolecular crystal quality research papers," Acta Crystallogr. Sect. B **56**, 868 (2000).
[10]V. Stojanoff, D. P. Siddons, L. A. Monaco, P. Vekilov, and F. Rosenberger, "X-ray topography of tetragonal lysozyme grown by the temperature-controlled technique," Acta Crystallogr. Sect. D **53**, 588 (1997).
[11]C. L. Caylor, I. Dobrianov, S. G. Lemay, C. Kimmer, S. Kriminski, K. D. Finkelstein, W. Zipfel, W. W. Webb, B. R. Thomas, A. A. Chernov, and R. E. Thorne, "Macromolecular Impurities and Disorder in Protein Crystals," Proteins **36**, 270 (1999).

[12]Z. W. Hu, Y. S. Chu, B. Lai, B. R. Thomas, and A. A. Chernov, "Diffraction and imaging study of imperfections of crystallized lysozyme with coherent X-rays," Acta Crystallogr. Sect. D **60**, 621 (2004).
[13]D. Lübbert, A. Meents, and E. Weckert, "Accurate rocking-curve measurements on protein crystals grown in a homogeneous magnetic field of 2.4 T," Acta Crystallogr. Sect. D **60**, 987 (2004).
[14]C. T. Putkunz, M. A. Pfeifer, A. G. Peele, G. J. Williams, H. M. Quiney, B. Abbey, K. A. Nugent, and I. McNulty, "Fresnel coherent diffraction tomography," Opt. Express **18**, 11746 (2010).
[15]X. Huang, R. Harder, S. Leake, J. N. Clark, and I. Robinson, "Three-dimensional Bragg coherent diffraction imaging of an extended ZnO crystal," J. Appl. Crystallogr. **45**, 778 (2012).
[16]W. Yang, X. Huang, R. Harder, J. N. Clark, I. K. Robinson, and H. K. Mao, "Coherent diffraction imaging of nanoscale strain evolution in a single crystal under high pressure," Nat. Commun. **4**, 1680 (2013).
[17]B. Abbey, "From grain boundaries to single defects: A review of coherent methods for materials imaging in the X-ray sciences," J. Miner. Met. Mater. Soc. **65**, 1183 (2013).
[18]N. W. Phillips, C. T. Putkunz, G. Van Riessen, H. D. Coughlan, M. W. M. Jones, and B. Abbey, "Ptychographic Fresnel coherent diffraction tomography at the nanoscale," Int. J. Mater. Res. **105**, 655 (2014).
[19]S. Boutet and I. K. Robinson, "Coherent X-ray diffractive imaging of protein crystals," J. Synchrotron Radiat. **15**, 576 (2008).
[20]A. Cole, "Absorption of 20-eV to 50,000-eV electron beams in air and plastic," Radiat. Res. **38**, 7 (2015).
[21]J. C. Falkner, A. M. Al-Somali, J. A. Jamison, J. Zhang, S. L. Adrianse, R. L. Simpson, M. K. Calabretta, W. Radding, G. N. Phillips, and V. L. Colvin, "Generation of size-controlled, submicrometer protein crystals," Chem. Mater. **17**, 2679 (2005).
[22]S. Boutet, L. Lomb, G. J. Williams, T. R. M. Barends, A. Aquila, R. B. Doak, U. Weierstall, D. P. DePonte, J. Steinbrener, R. L. Shoeman, M. Messerschmidt, A. Barty, T. A. White, S. Kassemeyer, R. A. Kirian, M. M. Seibert, P. a Montanez, C. Kenney, R. Herbst, P. Hart, J. Pines, G. Haller, S. M. Gruner, H. T. Philipp, M. W. Tate, M. Hromalik, L. J. Koerner, N. van Bakel, J. Morse, W. Ghonsalves, D. Arnlund, M. J. Bogan, C. Caleman, R. Fromme, C. Y. Hampton, M. S. Hunter, L. C. Johansson, G. Katona, C. Kupitz, M. Liang, A. V Martin, K. Nass, L. Redecke, F. Stellato, N. Timneanu, D. Wang, N. A. Zatsepin, D. Schafer, J. Defever, R. Neutze, P. Fromme, J. C. H. Spence, H. N. Chapman, and I. Schlichting, "High-resolution protein structure determination by serial femtosecond crystallography," Science **337**, 362 (2012).
[23]S. J. Leake, M. C. Newton, R. Harder, and I. K. Robinson, "Longitudinal coherence function in X-ray imaging of crystals," Opt. Express **17**, 15853 (2009).
[24]R. B. G. Ravelli and S. M. Mcsweeney, "The "fingerprint" that X-rays can leave on structures," Structure **8**, 315 (2000).
[25]W. P. Burmeister, "Structural changes in a cryo-cooled protein crystal owing to radiation damage," Acta Crystallogr. Sect. D **56**, 328 (2000).
[26]R. B. G. Ravelli, P. Theveneau, S. McSweeney, and M. Caffrey, "Unit-cell volume change as a metric of radiation damage in crystals of macromolecules," J. Synchrotron Radiat. **9**, 355 (2002).
[27]J. Murray and E. Garman, "Investigation of possible free-radical scavengers and metrics for radiation damage in protein cryocrystallography," J. Synchrotron Radiat. **9**, 347 (2002).
[28]R. Müller, E. Weckert, J. Zellner, and M. Drakopoulos, "Investigation of radiation-dose-induced changes in organic light-atom crystals by accurate d -spacing measurements," J. Synchrotron Radiat. **9**, 368 (2002).
[29]J. M. Holton and K. A. Frankel, "The minimum crystal size needed for a complete diffraction data set," Acta Crystallogr. Sect. D **66**, 393 (2010).
[30]R. Sanishvili, D. W. Yoder, S. B. Pothineni, G. Rosenbaum, S. Xu, S. Vogt, S. Stepanov, O. Makarov, S. Corcoran, R. Benn, V. Nagarajan, J. L. Smith, and R. F. Fischetti, "Radiation damage in protein crystals is reduced with a micron-sized X-ray beam," Proc. Natl. Acad. Sci. U.S.A. **108**, 6127 (2011).
[31]J. W. Murray, E. F. Garman, and R. B. G. Ravelli, "X-ray absorption by macromolecular crystals: The effects of wavelength and crystal composition on absorbed dose," J. Appl. Crystallogr. **37**, 513 (2004).
[32]J. N. Clark, L. Beitra, G. Xiong, A. Higginbotham, D. M. Fritz, H. T. Lemke, D. Zhu, M. Chollet, G. J. Williams, M. Messerschmidt, B. Abbey, R. J. Harder, A. M. Korsunsky, J. S. Wark, and I. K. Robinson, "Ultrafast three-dimensional imaging of lattice dynamics in individual gold nanocrystals," Science (New York, N.Y.) **341**, 56 (2013).
[33]C. A. Schneider, W. S. Rasband, and K. W. Eliceiri, "NIH Image to ImageJ: 25 years of image analysis," Nat. Methods **9**, 671 (2012).
[34]R. Gerchberg and W. Saxton, "A practical algorithm for the determination of phase from image and diffraction plane pictures," Optik **35**, 237 (1971).
[35]D. R. Luke, "Relaxed averaged alternating reflections for diffraction imaging," Inverse Problems **21**, 37 (2005).
[36]S. Marchesini, H. He, H. N. Chapman, A. Noy, M. R. Howells, U. Weierstall, and J. C. H. Spence, "X-ray image reconstruction from a diffraction pattern alone," Phys. Rev. B **68**, 140101 (2003).
[37]B. Ziaja, D. Van Der Spoel, A. Szoke, and J. Hajdu, "Auger-electron cascades in diamond and amorphous carbon," Phys. Rev. B **64**, 21404 (2001).
[38]B. Ziaja, A. Szöke, D. van der Spoel, and J. Hajdu, "Space-time evolution of electron cascades in diamond," Phys. Rev. B **66**, 24116 (2002).
[39]C. Caleman, G. Huldt, F. R. N. C. Maia, C. Ortiz, F. G. Parak, J. Hajdu, D. van der Spoel, H. N. Chapman, and N. Timneanu, "On the feasibility of nanocrystal imaging using intense and ultrashort X-ray pulses," ACS Nano **5**, 139 (2011).
[40]S. Boutet and I. K. Robinson, "Radiation driven collapse of protein crystals," J. Synchrotron Radiat. **13**, 1 (2006).
[41]N. Shimizu, K. Hirata, K. Hasegawa, G. Ueno, and M. Yamamoto, "Dose dependence of radiation damage for protein crystals studied at various X-ray energies," J. Synchrotron Radiat. **14**, 4 (2007).
[42]S. Banumathi, P. H. Zwart, U. A. Ramagopal, M. Dauter, and Z. Dauter, "Structural effects of radiation damage and its potential for phasing," Acta Crystallogr. Sect. D **60**, 1085 (2004).
[43]V. Guez, P. Roux, A. Navon, and M. E. Goldberg, "Role of individual disulfide bonds in hen lysozyme early folding steps," Protein Sci. **11**, 1136 (2002).